

Fast marching subjected to a vector field–path planning method for mars rovers

Santiago Garrido, Luis Moreno, Fernando Martín*, David Álvarez

Robotics Lab, Carlos III University of Madrid, Spain



ARTICLE INFO

Article history:

Received 26 October 2016

Revised 24 January 2017

Accepted 9 February 2017

Available online 14 February 2017

Keywords:

Path planning

Fast Marching

Planetary exploration

Mars rovers

ABSTRACT

Path planning is an essential tool for the robots that explore the surface of Mars or other celestial bodies such as dwarf planets, asteroids, or moons. These vehicles require expert and intelligent systems to adopt the best decisions in order to survive in a hostile environment. The planning module has to take into account multiple factors such as the obstacles, the slope of the terrain, the surface roughness, the type of ground (presence of sand), or the information uncertainty. This paper presents a path planning system for rovers based on an improved version of the Fast Marching (FM) method. Scalar and vectorial properties are considered when computing the potential field which is the basis of the proposed technique. Each position in the map of the environment has a cost value (potential) that is used to include different types of variables. The scalar properties can be introduced in a component of the cost function that can represent characteristics such as difficulty, slowness, viscosity, refraction index, or incertitude. The cost value can be computed in different ways depending on the information extracted from the surface and the sensor data of the rover. In this paper, the surface roughness, the slope of the terrain, and the changes in height have been chosen according to the available information. When the robot is navigating sandy terrain with a certain slope, there is a landslide that has to be considered and corrected in the path calculation. This landslide is similar to a lateral current or vector field in the direction of the negative gradient of the surface. Our technique is able to compensate this vector field by introducing the influence of this variable in the cost function. Because of this modification, the new method has been called Fast Marching (subjected to a) vector field (FMVF). Different experiments have been carried out in simulated and real maps to test the method performance. The proposed approach has been validated for multiple combinations of the cost function parameters.

© 2017 Elsevier Ltd. All rights reserved.

1. Introduction

The study of robot motion in rovers used for exploration in Mars or asteroids (Ceres, Vesta) has special difficulties because it is necessary to take into account multiple variables such as the obstacles, the changes in height, the slope of the terrain, the surface roughness, the uncertainty of the measurements, the composition of the ground (proportion of sand), possible small landslides due to the sand, and even the insolation level at each point of the path in order to increase the duration of the batteries. Some of these characteristics (slope, roughness, height) present scalar values, but others (landslides due to the sand) have to be represented by vectorial parameters.

The path planning problem for a mobile robot operating in environments with unknown obstacles (dynamic or not) consists of computing a collision-free trajectory from an initial point to a goal location. The planning module has to optimize its performance depending on the objectives of the vehicle. Different parameters can be used to check the behavior of the system. For example, the smoothness of the path, the system safety, and the gradient or slope are important when navigating outdoors.

In this paper, we have examined how to implement a path planner for a rover that is exploring Mars. These vehicles need expert and intelligent systems to make the best choices in order to survive on a hostile planet. The method has to consider the available information and the factors that influence navigation to compute the most adequate paths.

The Mars height map¹ (Fig. 1) obtained by the Mars Orbiter Laser Altimeter (MOLA), an instrument aboard NASA's Mars Global

* Corresponding author.

E-mail addresses: s Garrido@ing.uc3m.es (S. Garrido), moreno@ing.uc3m.es (L. Moreno), fmmonar@ing.uc3m.es (F. Martín), dasanche@ing.uc3m.es (D. Álvarez).

¹ <http://mola.gsfc.nasa.gov/topography.html>.

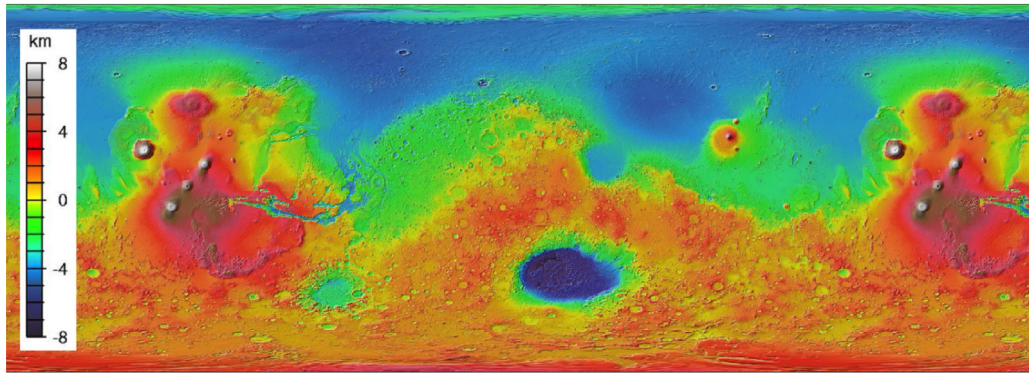


Fig. 1. Mars height map. Size: 46,080 × 23,040 pixels; Scale: 1: 25, 000, 000. Projection: −180E to 180E, 90N to −90N.

Surveyor, is the source of information that is used to compute the robot's path. The best paths will be calculated over zones of this map depending on different variables. Different factors have to be considered according to the type of environment where the method will be applied. In our approach, these factors are classified into scalar and vectorial variables. In order to introduce these characteristics in the path planning module, a technique that optimizes a scalar cost function subjected to an external vector field is proposed. Due to our previous experience (Garrido, Moreno, Abderrahim, & Blanco, 2009; Garrido, Moreno, & Blanco, 2008; Valero-Gómez, Gómez, Garrido, & Moreno, 2013), we have chosen the Fast Marching (FM) method (Sethian, 1996) as the basis of the path planner. A modified version called Fast Marching (subjected to a) vector field (FMVF) has been implemented in this work to deal with factors that can be represented by scalar parameters and an external vector field.

This paper investigates how to apply the FMVF algorithm in different situations to obtain optimal paths for Mars rovers, but it is possible to extrapolate the same technique to other vehicles used for space exploration on planets and asteroids.

This new method consists of several steps. First, a map of the environment is created using the available information. After that, the cost or potential of each location has to be computed. Finally, the optimal path is calculated applying the FMVF method. These steps are introduced below.

The input data is the point cloud of the surface. This cloud can proceed from the rover laser sensor, from a known map, or from a mixture of both sources of information. The Mars height map is used here, but the algorithm is not limited to this option. The initial map is discretized in an orthogonal grid. As will be explained in Section 3, the planning algorithm can be applied to the initial map or to a three-dimensional triangular mesh that represents more accurately the planet's surface.

Although any scalar property could be taken into account, the change with respect to the initial height, the slope of the terrain, and the surface roughness are extracted in this work to build the scalar component of the cost value. These parameters can consider the robot's limitations (characteristics and environment conditions) to generate a cost value for each cell of the map. As will be described in Section 4, the slope or the roughness can be saturated to reduce the speed to the minimum when navigating hazardous areas. Besides, the FM method returns smooth paths, which is helpful when applied to nonholonomic vehicles. This cost value can be viewed as a difficulty or viscosity map which is situated on the planet's surface. Once the cost value is computed for the whole grid, the method is ready to apply the FM algorithm over the surface to generate the path. In other words, the initial map is modified and a potential is given to each cell. The potential field represents the influence of the scalar properties.

Without using the new potentials, the shortest path between two points would be obtained (i.e., the geodesic distance). When the potential with the scalar properties is included, the path considers the features of the surface and the limitations of the robot. Moreover, it gives us information about the speed of the robot based on the FM wave propagation speed (Garrido et al., 2009).

One of the crucial problems of the Mars rovers when navigating is caused by the presence of sand on the ground. This sand can produce two different phenomena. First, sand banks in which it is better not to enter could be formed in specific zones. In this case, these areas could be classified as dangerous terrain using a scalar parameter. This variable could be included in the previously explained scalar component of the cost function. Second, small landslides can change the position and direction of the previously calculated trajectory. The current approach models these lateral currents by using an external vector field that is also included in the cost of the planning module. This idea relies on the solution published in Petres et al. (2007). In this way, the planning method is based on a cost function that combines scalar and vectorial properties.

The path planning method has been tested using simulated and real input data. The objective is to demonstrate that the proposed strategy is a suitable technique and it takes into account the most typical factors that could influence navigation on the surface of Mars. Since different parameters can be introduced in the cost function, the experiments will validate our method under different circumstances that result in different cost functions. Smooth and safe paths are obtained in all cases.

This paper is organized as follows. The state of the art is reviewed in Section 2. Section 3 details the implementation of the FM method. After that, the FMVF algorithm is explained in Section 4. The experimental results are presented in Section 5 and, finally, the most important conclusions are summarized in Section 6.

2. State of the art

Path planning is one of the most widely studied problems in robotics. It consists of finding a path from an initial point to a goal location. The most typical algorithms are reviewed in this section. There are multiple methods that have been successfully applied and classifications depending on the objectives followed by the planner. For example, a classic approach classifies the algorithms according to the completeness, which means that the planning method would find a path if it existed. The increase of the computing power makes it possible to consider many different challenging goals such as the optimization of the path length or the safety.

An interesting division is proposed by LaValle (2011). Two groups of algorithms are defined depending on how the informa-

Table 1

Path planning: Most common algorithms and characteristics.

Algorithm	Search algorithm (Dijkstra, A*)	Advantages	Limitations
Combinatorial planning	Not required	Complete	Suboptimal paths (not smooth) Worse for HD spaces
Grid map	Required	Complete	Suboptimal paths (not smooth) Worse for HD spaces
Sampling-based (RRT, PRM)	Required	Probabilistically complete	Suboptimal paths
Potential fields (FM)	Not required	Better for HD spaces Complete Optimal paths (smooth)	(not smooth) Local minima (not in recent versions) Worse for HD spaces

tion is processed. The first group is named “combinatorial planning”. In these methods, all the information that is needed by the planning algorithm is used to construct a structure (Berg, Kreveld, Overmars, & Schwarzkopf, 2000; LaValle, 2006). The path is computed according to the structure. Some examples are visibility graphs, Voronoi diagrams, and cell decomposition. The second option is to apply a sampling-based approach to incrementally compute the solution in the search space utilizing a collision-detection system (LaValle, 2006). This group of techniques is more adequate for high-dimensional (HD) spaces because it is not necessary to compute the whole space and the execution time is less affected by the number of dimensions.

Many different techniques can be cited. In the Probabilistic Road Maps (PRM) (Kavraki, Svestka, Latombe, & Overmars, 1996), a set of random samples (checking if they belong to the free space) forms the roadmap where the path is estimated. The Rapidly exploring Random Tree (RRT) (Kuffner & LaValle, 2000) is a very common solution that is based on the creation of branches in a tree that represents possible paths. It is necessary to check the collisions in the tree until a path between the initial and the goal point is reached. A different option is to build a grid map where classic search algorithms (Dijkstra, A*) compute the best paths. In the potential field-based techniques (Barraquand, B., & Latombe, 1992), the main idea is to consider that the robot is influenced by a potential field. A traditional shortcoming related to the potential fields is the presence of local minima. However, they have evolved to solutions where local minima are avoided. For example, Ge and Cui (2000) take into account the distance to the goal to implement a potential field which ensures that the goal position is reached. The algorithm proposed in this paper can be included in this class. The FM method is a numerical algorithm based on a potential field that was introduced by Sethian (1996). An artificial potential field is created according to the information provided by sensors. Local minima are avoided because the algorithm relies on a wave expansion that can cover the whole map. The main features of the most common algorithms are summarized in Table 1.

In the original version of FM, each cell of the grid has an isotropic behavior. The vector field that has been included to represent phenomena like sand landslides introduces an anisotropic behavior in the planning module.

Different authors have studied the influence of the anisotropy in path planning. Sethian and Vladimirs (2003) introduced a set of techniques called ordered upwind methods for approximating the solution of general Hamilton–Jacobi partial differential equations. They use partial information about the characteristic directions to decouple these nonlinear systems, reducing the computational effort with respect to the previous techniques. In Bougleux, Peyré, and Cohen (2008); Peyré (2010), the authors have considered 2D Riemannian manifolds defined over a compact planar domain and have designed an anisotropic tensor field that

corresponds to a Riemannian metric in order to locally impose the orientation and aspect ratio of the solution. Faster strategies were proposed in Jbabdi et al. (2008); Shum, Morris, and Khajepour (2015). In Petres et al. (2007); Petres, Pailhas, Petillot, and Lane (2005), the same name, anisotropic FM (AFM), is used for different solutions of a similar problem. The names directional FM and FM* have been utilized in Pardeiro (2015) for oriented propagation algorithms based on FM.

2.1. Planet exploration

Multiple researchers have investigated how to apply different versions of the previous techniques to planet exploration.

Volpe, Estlin, Laubach, Olson, and Balarlam (2000) have implemented navigation techniques addressing this problem at multiple levels. Their method computes local paths up to the range of the distance sensors. Their planner is based on the work presented in Laubach and Burdick (1999). This algorithm has two operating modes: motion to goal or boundary following. Different subgoals are defined and the sensor information is used to decide if the vehicle goes to the objective or if it is necessary to avoid an obstacle. This technique does not return smooth paths and it only takes into account the presence of obstacles in the scanning area.

An overview of the mobility and the vision capabilities of the NASA's Mars rovers is given in Maimone, Leger, and Biesadecki (2007). The local path selection mode makes it possible to correct the initial path. The authors have reported that visual odometry and a clever sequence of commands are needed to navigate safely on high slopes or in sandy areas. The local obstacle avoidance module is called GESTALT (Grid-based Estimation of Surface Traversability Applied to Local Terrain). This system uses stereo cameras to evaluate terrain safety and avoid obstacles. The onboard path planning method has been presented in Carsten, Rankin, Ferguson, and Stentz (2007). The global planner depends on the Field D* algorithm (Ferguson & Stentz, 2006). Field D* is a grid-based algorithm that applies interpolation to generate direct, low cost paths. A cost that represents the traversability is given to each cell and the objective is to minimize the cost between two locations.

Gennery (1999) has studied the traversability based on three-dimensional data. This parameter is computed taking into account the slope, the height, and the surface roughness. The author has proposed a planning method that relies on the minimization of a cost function that uses both the distance traveled and the traversability.

Rekleitis, Bedwani, Dupuis, and Allard (2008) have presented the path planning approach adopted by the Canadian Space Agency. The map information is encoded to generate a graph structure where the path planning task corresponds to a graph search in which different objectives can be followed depending on a cost

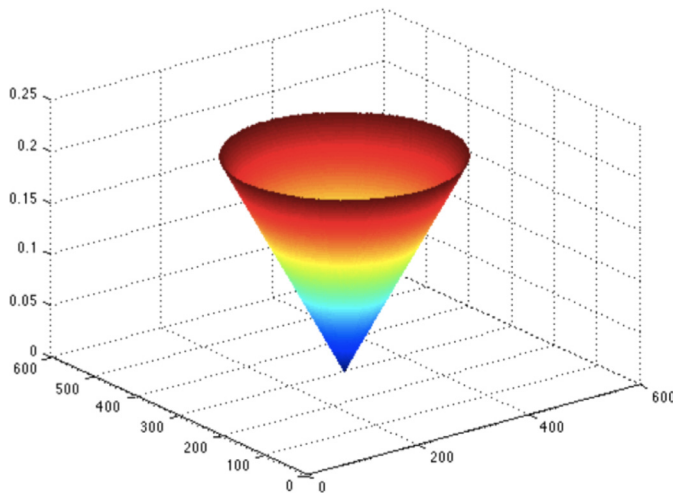


Fig. 2. Wave expansion when the refractive index is constant. Time in the third axis. Units in cells and seconds.

function that has to be defined. They consider distance, slope, roughness, and cell count.

In Ishigami, Nagatani, and Yoshida (2007), dynamic simulations are implemented to choose between different paths. The authors compare the stability, the wheel slippage, the elapsed time, and the energy consumption.

Potiris, Tompkins, and Goktogan (2014) have followed a strategy based on PRM where a parameter called *terrain sensitivity* is used to represent significant slopes and rough terrain.

Muñoz, Rodríguez, Castaño, and Martínez (2012) have proposed a metric to avoid large heading changes. They have concluded that paths with more turns could be convenient when shorter paths have abrupt direction changes.

3. The Eikonal equation and the fast marching method

A desirable feature for an exploratory vehicle is to drive in a smooth, safe, and fast way to the goal point. The electromagnetic waves have interesting properties that can be applied to solve the path planning problem. If there is an antenna located at the goal point that emits an electromagnetic wave, the robot could navigate to the destination following the waves to the source. This idea is especially interesting because the potential magnetic field has all the good properties desired for the path, which are smoothness and the absence of local minima. In a similar manner, Fermat's principle in optics says that the path of a beam of monochromatic light follows the path of least time. When the refractive index is constant, the wave fronts are circles which represent different arrival times and the paths are straight lines (Fig. 2, Fig. 3 left). When the refractive index varies continuously, the light beam is also continuously bent and smooth paths are obtained (Fig. 3 right).

One way to characterize the position of a front in expansion is to compute the arrival time T in which the front reaches each point of the space. It is straightforward that, for one dimension, the equation of the arrival function can be obtained in an easy way. The distance x is the product of the speed F and the time T . The spatial derivative of this equation is

$$\frac{dT(x)}{dx} = \frac{1}{F(x)}. \quad (1)$$

It can be noticed that the magnitude of the derivative of the arrival time function $T(x)$ is inversely proportional to the speed.

For multiple dimensions, the same concept is valid but the derivative is replaced by the gradient, because the gradient is orthogonal to the level sets of the arrival time function.

If the speed depends only on the position, the Eikonal equation is obtained:

$$|\nabla T(x)|F(x) = 1, \quad (2)$$

where x represents a spatial point of the map. The Eikonal equation can be solved for each point of the environment, which is given by the planet's surface in this approach.

The FM technique is an algorithm developed by Sethian (1996) to solve the Eikonal equation. The time complexity of this method is $O(n)$ (Yatziv, Bartesaghi, & Sapiro, 2006), where n is the number of cells of the map (the map is implemented in a discrete grid). The solution of the differential equation is based on an upwind finite-difference approximation to the gradient.

In the FM method, it is assumed that the cost value is always positive, which means that there are no reflections and the wave front is always moving forward. Under these conditions, the wave front crosses each point only once. In the basic version, since the speed is constant, the wave propagation results in a path that corresponds to the Geodesic distance (Fig. 3 left). The refraction index is the metric that indicates the velocity at which the wave front moves forward.

The speed or potential of each cell is not constant in the version implemented in this paper (Fig. 3 right). A potential field is built according to the velocities of each cell. $F(x)$ considers both scalar and vectorial properties that symbolize typical factors to be taken into account in Mars. The speed at each cell is dependent on the cost value that will be presented in Section 4. For this reason, F will represent the cost value given to each cell from now on.

Two different methods are used here to solve the Eikonal equation in orthogonal (Section 3.1) or triangular (Section 3.2) meshes. The orthogonal mesh corresponds to the grid map in two dimensions. The triangular mesh is built in three dimensions from the initial map in order to represent more accurately a three-dimensional surface. Experiments with both approaches have been conducted. Both implementations are based on previous research. A schematic description is given in the next sections. The reader can consult (Garrido et al., 2009) for a more detailed explanation.

3.1. Algorithm implementation in an orthogonal mesh

This section describes the implementation of the FM method in an orthogonal mesh. This technique is based on a wave front propagation normal to itself with a speed function $F(i, j)$, where (i, j) are the coordinates of the map. $T(i, j)$ is the time at which the wave crosses the point (i, j) . The times of arrival are calculated in an incremental way for the whole grid. After that, the planning method computes the path that minimizes the time of arrival using the gradient descent method.

While evolving, the algorithm classifies the points of the mesh into three sets: frozen, open, and unvisited. Frozen points are those ones where the arrival time has been computed. Unvisited points are those ones that have not been processed yet. The wave front is formed by the open points, which represent the boundary between frozen and unvisited regions.

At the beginning, the starting point is marked as frozen with time of arrival equal to zero. All points adjacent to it (von Neumann neighborhood is considered) are marked as open and their times of arrival are computed using the following equation (Osher & Sethian, 1988):

$$\left(\frac{T_{ij} - T_x}{\Delta x} \right)^2 + \left(\frac{T_{ij} - T_y}{\Delta y} \right)^2 = \frac{1}{F_{ij}^2}, \quad (3)$$

where T_x and T_y are the minimum arrival times of the neighbors in each axis, and F_{ij} is the velocity of propagation in the cell for which

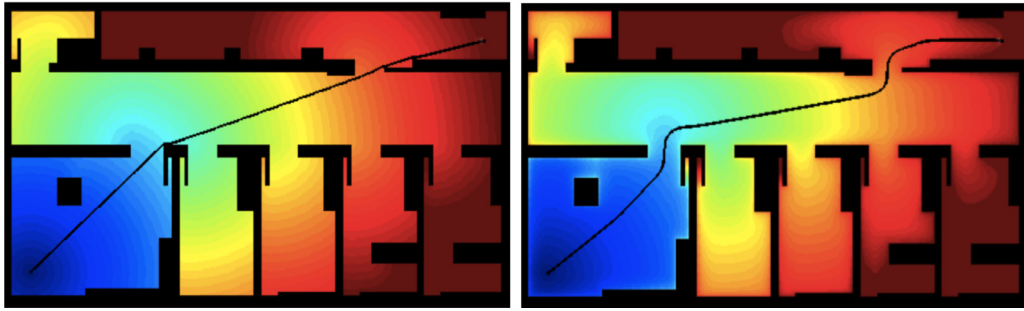


Fig. 3. FM examples: Left: Basic version with constant speed; Right: Repulsive potential field from obstacles.

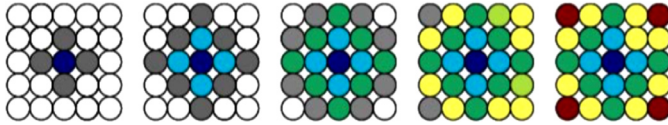


Fig. 4. FM propagation from an initial point. Constant refraction index. Iterations of FM with one wave in 2D. Color code: white (unvisited), dark blue (initial point), grey (open), other colors (frozen). Different colors represent different times of arrival. (For interpretation of the references to colour in this figure legend, the reader is referred to the web version of this article.)

the arrival time is being computed (a slightly different notation is used for simplicity, T_{ij} is $T(i, j)$ and F_{ij} is $F(i, j)$). The objective is to solve the equation obtaining T_{ij} for the current cell. The solution depends on the number of frozen points that are neighbors of the open point for which the front propagation is being calculated. Different strategies are needed for one or two frozen points. A detailed explanation of this method can be found in Valero-Gómez et al. (2013).

The procedure to compute the solution is detailed in pseudocode in [Algorithm 1](#). An example is given in [Fig. 4](#). At each it-

Algorithm 1 FM Method.

Require: A grid map X of size $m \times n$, source point x_0 .
Ensure: The grid map X with the T value set for all cells.

Initialization.

- 1: **for all** $x \in X$ **do**
- 2: $T(x) \leftarrow \infty$;
- 3: **end for**
- 4: $T(x_0) \leftarrow 0$;
- 5: $frozen \leftarrow x_0$;
- 6: $open \leftarrow \mathcal{N}(x_0)$; ▷ Neighbors of x_0 .
- 7: **UPDATE(open);** ▷ Time of arrival computed for open.

Iteration.

- 8: **while** $frozen \neq X$ **do**
- 9: $x_1 \leftarrow \arg \min_{x \in open} T(x)$;
- 10: **for all** $x_i \in \mathcal{N}(x_1) \notin frozen$ **do**
- 11: **UPDATE(x_i);** ▷ Time of arrival computed for all neighbors.
- 12: **end for**
- 13: $open \leftarrow open \cup \mathcal{N}(x_1) \notin frozen$; ▷ Updating sets.
- 14: $frozen \leftarrow frozen \cup \{x_1\}$;
- 15: **end while**

eration, the open point with the smallest value of T is labelled as frozen and its neighbors are analyzed and tagged as open. The process continues until all points are marked as frozen or the goal is reached. In the left part of the figure, the dark blue point is the starting point of the wave and its neighbors are marked in grey. In the second figure from the left, their times of arrival are com-

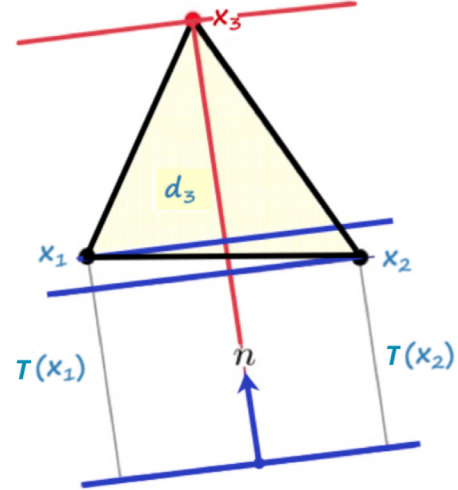


Fig. 5. FM update step applied to a triangle x_1, x_2, x_3 when the times of arrival corresponding to two vertices are known.

puted and they are colored in light blue, while their neighbors are labelled in grey. The algorithm continues and the points with the same time of arrival are marked with the same color. Finally, since the time of arrival function has a funnel-like shape (if the time of arrival is represented in a third dimension), the robot's path is extracted using the gradient descent method.

3.2. Algorithm implementation in a triangular mesh

Although FM was first described for orthogonal meshes, it was extended later to general triangular meshes since these structures are more flexible when describing surfaces (Kimmel & Sethian, 1998). This version requires two vertices of the same triangle in order to compute the time of arrival of the third vertex. In the example of [Fig. 5](#), the obtention of the time of arrival $T(x_3)$ for the triangle defined by x_1, x_2 and x_3 is analyzed. If it is considered that x_1 and x_2 and their times of arrival are known, the equations of the blue lines that cross these points are

$$a x_{11} + b x_{12} = d_1 = T(x_1), \quad (4)$$

$$a x_{21} + b x_{22} = d_2 = T(x_2), \quad (5)$$

where x_{11} and x_{12} are the two-dimensional coordinates of x_1 and d_1 represents the time of arrival. Observing the figure, the perpendicular direction (with respect to the blue lines) corresponds to the time of arrival. The coefficients a , b , and the normal vector n can be calculated by solving this system of equations. After that, the authors in Kimmel and Sethian (1998) use the following version of

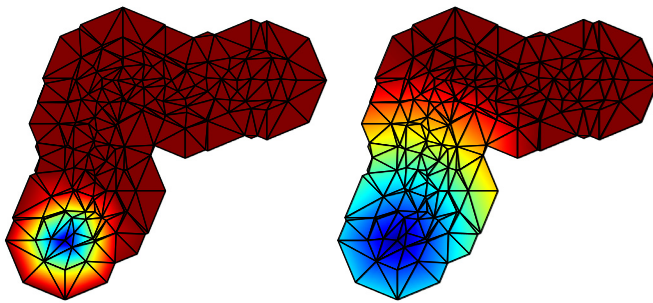


Fig. 6. FM front wave propagation in a triangular mesh. The source point is at the bottom.

the Eikonal equation to compute the value of x_3 :

$$\left(\frac{x_3 - x_1}{h}\right)^2 + \left(\frac{x_3 - x_2}{h}\right)^2 = \frac{1}{F_{x_3}^2}. \quad (6)$$

The solution is substituted in the equation of the red line to calculate the time of arrival of the third vertex:

$$d_3 = T(x_3) = a x_{31} + b x_{32}. \quad (7)$$

The aforementioned idea works for non-obtuse triangular meshes. If there are obtuse triangles in the mesh, it can be solved by connecting the vertex x_3 to another point of the mesh (Kimmel & Sethian, 1998). Fig. 6 depicts the front wave propagation in a triangular mesh. The general FM algorithm can still be applied in this case, with the only change of the update step.

4. Fast Marching Method subjected to a Vector Field

The objective of this technique is to compute a path according to the type of environment where the method will be applied. The factors to be considered in Mars can be classified into scalar and vectorial properties. In order to introduce these characteristics in the path planning module, an algorithm that optimizes a scalar cost function subjected to an external vector field is proposed.

The original FM method considers a grid map where the potential is constant for the free space. In this paper, the potential is modified to define a value F_{ij} for the potential field of each cell that includes the desired parameters. Following this idea, the potential field is described by the next equation:

$$F_{ij} = F_{scal,ij} + F_{vect,ij}, \quad (8)$$

where F_{scal} and F_{vect} represent the influence of the scalar and the vectorial properties, respectively. Both types of features are introduced in a cumulative way following the same approach proposed in Petres et al. (2007). Different weights could be given to each component if necessary.

Once the cost values are calculated for the whole map (F_{ij} can be viewed as a cost value), the FM method computes the shortest path in the potential field using the gradient decent method. This is a general technique and any other strategy could be applied. If F_{ij} is normalized according to the maximum speed of the Mars rover, the optimal path could be estimated for the vehicle of interest.

The scalar properties extracted from the map that are computed by the planner are the changes in height, the slope, and the spherical variance, which is a parameter that gives us information about the surface roughness. These data can take into account the robot's characteristics and the environment conditions to generate weights (F_{scal}) with the cost values for each location (Section 4.2). For example, the slope or the roughness can be set up to reduce the speed to the minimum when navigating dangerous areas. This set of weights can be viewed as a difficulty or viscosity map. Once the weights are calculated, the FM algorithm could be applied over

the modified potential field to generate the path. Nevertheless, the scalar properties are not the only ones that are taken into account by the cost function.

Moreover, the planning method is subjected to an external vector field to represent phenomena like sand landslides. This vector field, which will be explained later in this section, introduces an anisotropic behavior in the planning module. In the original version of FM, each cell of the grid has an isotropic behavior. The wave expansion has to be considered in a different way in an anisotropic cost map.

The idea presented in Petres et al. (2007) is modified in this paper to develop the vectorial component of the cost function. For this reason, the term "subjected to a vector field" is an adequate name to represent the physical meaning of the FMVF planning technique.

It has to be said that, to the best of our knowledge, the authors did not continue using the technique published in Petres et al. (2007, 2005). A possible shortcoming of their method is that they normalize the magnitude of the external vector field without taking into account the scalar component of the cost function. This causes that two vector fields with different intensities (for example, one and ten) have the same effect on the final path. The real influence of the vector field is not introduced in the cost map. The function that is normalized in this paper is the total cost function given by Eq. (8). Each component of this equation is described in the next sections.

4.1. Cost value of the external vector field

The influence of an external factor represented by a vector field on the velocity of a vehicle depends on the magnitude of both variables and the angle between them. If this relation is defined by the dot product of the gradient of the time of arrival and the external vector field, the next equation can be applied to measure this factor:

$$F_{vect,ij} = \langle \nabla T(i, j), \vec{F}_{ext,ij} \rangle, \quad (9)$$

where $\langle \cdot, \cdot \rangle$ is the standard dot product in \mathbb{R}^2 . $\vec{F}_{ext,ij}$ is the external vector field and $F_{vect,ij}$ is the component to be added to the cost function. This formula can be modified to change the influence of the vector field.

Analyzing Eq. (9), the force favors the vehicle when both the external vector field and the vehicle are pointing to the same direction. In this way, vectorial features can be included in the planning method. This idea is based on the solution proposed in Petres et al. (2007). However, the vector field is not limited here by a weight factor. In the AFM approach, the vector field component is normalized and, after that, it is added to the scalar term of the cost value. The total cost value is normalized in the FMVF method, which is believed to be a better option when modeling the influence of phenomena that can be found in Mars. The notation is slightly different because it has been adapted to the current method. More details on the algorithm can be consulted in Petres et al. (2007).

It is important to highlight that the new cost function defined in Eq. (8) must be always positive, because the wave front cannot move backwards in the FM method.

The influence of an external vector field is illustrated in Fig. 7. There is a rectangular obstacle in the middle. The expansion of the wave without an external vector field is shown in the left part of the figure. In the right part, the expansion is influenced by an external unitary vector field which is pointing to the right in the upper part of the map and to the left in the lower part.

The wave expands faster in the upper part. Furthermore, the FMVF algorithm can include multiple scalar properties in the cost value. These characteristics are described in the next section.

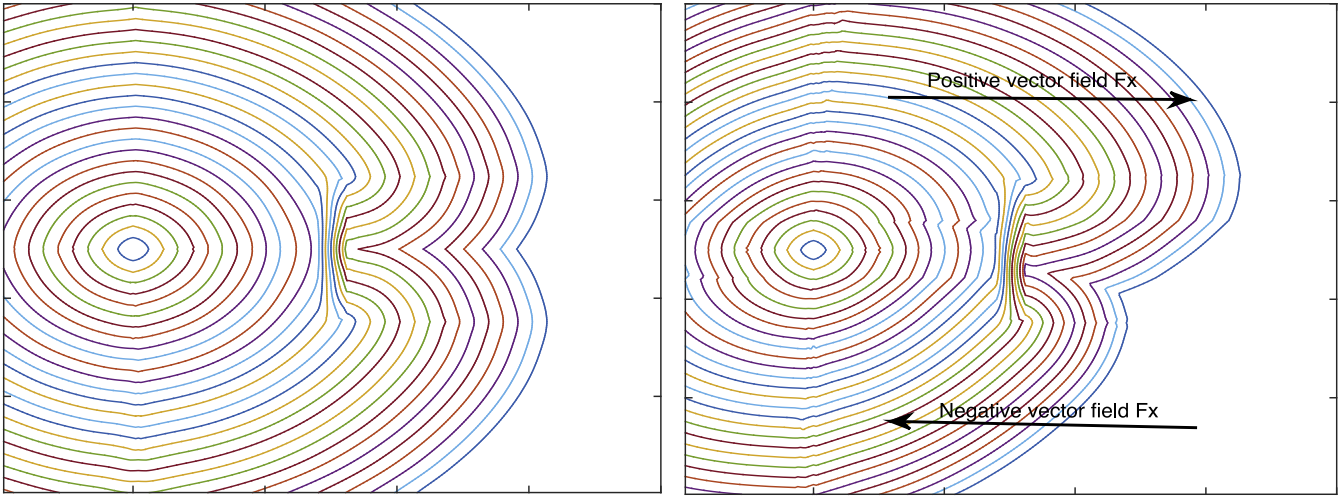


Fig. 7. Left: FM expansion wave with a rectangular obstacle in the middle; Right: FMVF expansion wave subjected to a unitary vector field that is pointing to the right in the upper part and to the left in the lower part.

4.2. Cost value of the scalar properties

Multiple scalar variables can be introduced in the cost function of the path planning method. The main objective is to define a cost value for each cell $F_{scal,ij}$. The current approach is based on the weighted sum of the parameters. The surface roughness, the slope of the terrain, and the changes in height with respect to the initial point of the path are the variables that will be included in the scalar cost value. Each component of the scalar cost is explained in the following paragraphs.

In [Castejón, Boada, Blanco, and Moreno \(2005\)](#), an equation to calculate the roughness degree is presented. The spherical variance finds the roughness of a surface to determine the level of difficulty for the vehicle to move through it. The spherical variance is obtained from the orientation variation of the normal vector at each point. In a uniform terrain (low roughness), the normal vectors will be approximately parallel and, for this reason, they will present a low dispersion. In an uneven terrain (high roughness), the normal vectors will present a great dispersion due to changes in their orientation. The spherical variance is obtained using the available sensor data following the next simple procedure.

Given a set of n normal vectors to a surface (unitary vectors) defined by three Cartesian coordinates (x_i, y_i, z_i) (extracted from the Mars height map in this case), the module of the sum vector is

$$R = \frac{1}{n} \sqrt{\left(\sum_{i=0}^n x_i \right)^2 + \left(\sum_{i=0}^n y_i \right)^2 + \left(\sum_{i=0}^n z_i \right)^2}, \quad (10)$$

where it can be noticed that the mean value is normalized ($R \in [0, 1]$).

The spherical variance S_v is the complementary of the previous result:

$$S_v = 1 - R. \quad (11)$$

When $S_v = 1$, there exists a maximum dispersion that can be considered as the maximum roughness degree. When $S_v = 0$, a full alignment exists and the terrain is flat.

The slope of the terrain (S_t) is also an important factor. This parameter can be normalized or even saturated depending on the robot's capabilities. The saturation of this variable consists of defining a maximum threshold for the gradient. The maximum inclination that the rover is able to cross will be the limit value for the saturated gradient. In this way, S_t can be penalized in order to

avoid the saturated zones. The other scalar variables could also be saturated if necessary.

The last parameter is the change in height (H_c) with respect to the initial point of the path. The objective is to drive on flat surfaces, and values close to the initial one are favored.

As previously explained, the scalar properties are used to compute the scalar component of the cost value that modifies the path given by the original FM method. These characteristics can be combined in different ways in order to satisfy different requirements. In addition, any other feature defined by a scalar value could be added. For example, an interesting property that could be included is the solar energy. The objective of the planner could be to maximize the energy absorption. This parameter depends on the inclination of the solar panels.

In this paper, the slope, the spherical variance, and the change with respect to the initial height are computed for each point of the map. A weighted sum of these variables is applied to obtain the scalar cost of the FMVF method:

$$F_{scal,ij} = 1 - (a_1 \cdot S_{v,ij} + a_2 \cdot S_{t,ij} + a_3 \cdot H_{c,ij}), \quad (12)$$

where a_1, a_2 and a_3 are weights ($\sum_i a_i = 1$). $F_{scal,ij}$ can be limited according to the navigation requirements.

[Eq. \(12\)](#) is normalized to be in the interval $[0, 1]$. Different values can be given to a_1, a_2, a_3 in order to favor or penalize particular situations depending on the task requirements. $F_{scal,ij} = 1$ corresponds to points with maximum speed. Locations with $F_{scal,ij} = 0$ are places with minimum speed. This means that the robot will not be able to pass across them.

When F_{ij} is generated for the whole map, the FMVF algorithm is run to calculate the best path. With the FMVF technique, it can be assured that the path will take into account the desired parameters. Different examples are given in [Section 5](#) to validate the current approach.

5. Experimental results

Different tests have been carried out to check the performance of the FMVF algorithm. First, several examples are given in a simulated environment to examine the influence of an external vector field. Since different parameters can be introduced in the cost function of the planning module, the next experiments validate our method under different circumstances that result in different cost values in order to highlight particular situations that can occur in

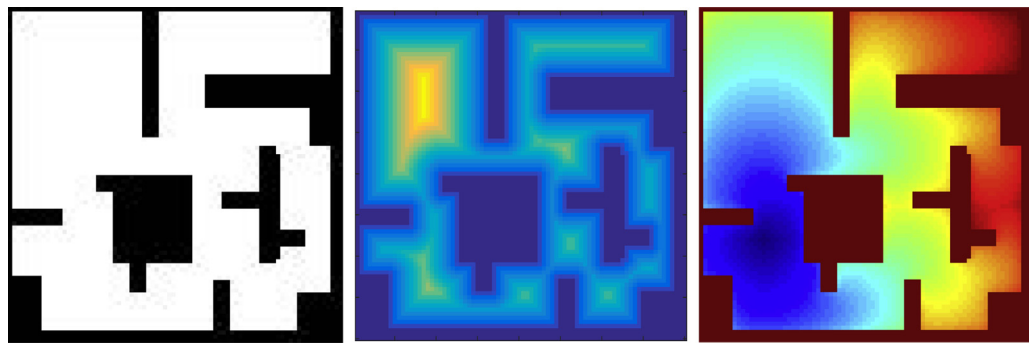


Fig. 8. Left: Simulated indoor map. White for free space and black for obstacles. Size: 80×80 cells. Middle: Distance to te closest obstacle ($F_{scal,ij}$), computed from zero (dark blue) to one (yellow). Right: Times of arrival for each cell ($F_{vect,ij} = 0$). Times from blue (initial point) to red (goal). (For interpretation of the references to colour in this figure legend, the reader is referred to the web version of this article.)

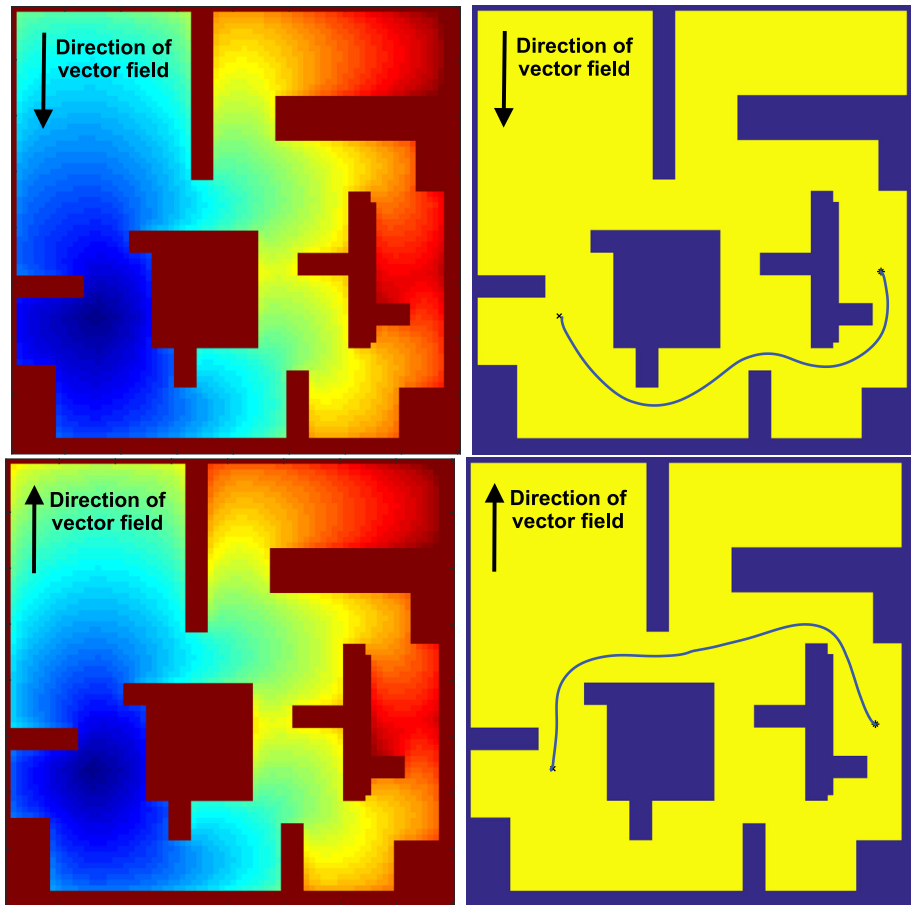


Fig. 9. Example of the FMVF method in a simulated indoor map. Top: Times of arrival for each cell (left) and path (right) with a constant vector field that is pointing down. Bottom: Times of arrival for each cell (left) and path (right) with a constant vector field that is pointing up. Times from blue (initial point) to red (goal). (For interpretation of the references to colour in this figure legend, the reader is referred to the web version of this article.)

Mars. The last experiments study an option that permits to avoid certain zones.

5.1. Validation in a simulated environment

The first experiments show the influence of an external vector field on the path planning module. In order to do that, two simple tests in a simulated environment are proposed. Orthogonal meshes are used in both cases.

A simulated map of an indoor environment is displayed in Fig. 8. The grid map is formed by obstacles (black) and free places (white). In order to apply the FMVF method, $F_{scal,ij}$ is the distance

to the closest obstacle in this experiment (middle part of Fig. 8). A normalization factor is included. $F_{scal,ij}$ varies from zero (dark blue) to one (yellow). The formula given in Eq. (12) is not considered because the map has not enough information (plane, same properties in the whole grid). The objective is to illustrate the influence of an external vector field. The times of arrival when $F_{vect,ij} = 0$ are shown in the right part of the figure.

Fig. 9 details the behavior of the FMVF method for two external vector fields. The algorithm obtains the propagation of a wave from the initial point given the scalar potential when an external vector field is also applied. Unitary fields are added in this case. The times of arrival according to the total cost values (F_{ij}) when the vector

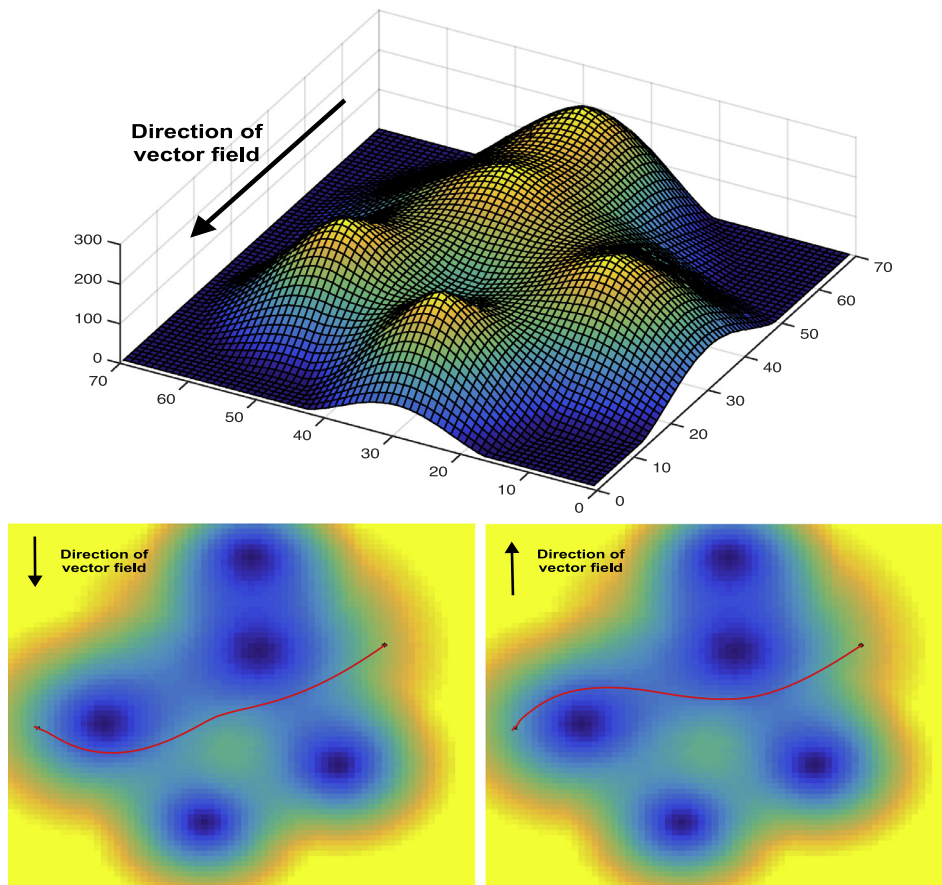


Fig. 10. Example of the FMVF method in a simulated map that represents a three-dimensional surface. Top: Simulated map. Units in cells. The direction of the vector field (corresponding to the bottom left image) is indicated. Bottom left: path when the vector field is pointing down. Bottom right: path when the vector field is pointing up.

field is pointing down and when it is pointing up are shown in the left part of the figure. Finally, it is possible to find the paths by applying the gradient decent method (right part of Fig. 9).

The influence of the vector field can be appreciated in the figure. Different ways are followed in each case. It can also be observed that the path is not close to the obstacles. The planning method maintains the smoothness and the safety, characteristics that are reported in our previous work.

The next experiment includes an additional variable which penalizes the path depending on the change with respect to the initial height. This is an interesting feature for rovers.

If the height change is considered as a difficulty, the reference height has to be computed for the initial point and changes with respect to the reference have to be penalized. In this case, $F_{scal, ij}$ is equal to H_{cij} . Only one scalar parameter is taken into account.

The simulated map of Fig. 10 represents a three-dimensional view of a planet's surface. Two different paths for two different external vector fields (also unitary) are computed. The vector field points down (in the horizontal projections shown at the bottom, it does not depend on the height) in the left part of the figure. In the right part, it points up. In both paths, it can be observed that the changes in height are minimum due to the penalization factor introduced in the cost function. Both paths are smooth and safe.

5.2. Experiments in real map

Information about the planet's surface is needed to apply the current technique in real conditions. The Mars height map provided by the NASA is used in this paper (Fig. 1). The map resolution is 60 km at the equator. An area surrounding the Gale

Crater, where Curiosity landed on Mars², has been chosen for the experiments. The crater has a diameter equal to 154 km. The zone map has been discretized to a 600×600 grid where the planning method needs less than 0.1 seconds to compute the path in all cases.

The objective is to test the method under different circumstances. Several paths have been computed and different values have been given to the weights presented in Section 4 in order to examine different situations that can occur when the Mars rover is navigating. These experiments are presented in the next sections.

5.2.1. Influence of landslides

One of the main objectives of this paper is to improve the robot's capabilities in surfaces with landslides. The presence of sand banks and landslides is one of the biggest problems of Mars rovers when navigating. Sand banks can be avoided by penalizing $F_{scal, ij}$ in the desired zones. Landslides can be modeled by an external vector field. Two different tests have been performed to examine this parameter. The use of a non-constant vector field that depends on the gradient is explored in both cases.

If the influence of sand landslides over the surface of Mars is analyzed, this variable can be characterized by an external vector field that is proportional to the gradient of the surface. More pronounced slopes will cause more movement of sand.

In the first experiment, Eq. (9) is modified to minimize the influence of landslides:

$$F_{vect, ij} = 1 - \langle \nabla T(i, j), \vec{F}_{ext, ij} \rangle. \quad (13)$$

² <http://mars.nasa.gov/msl/mission/timeline/prelaunch/landingsiteselection/aboutgalecrater/>

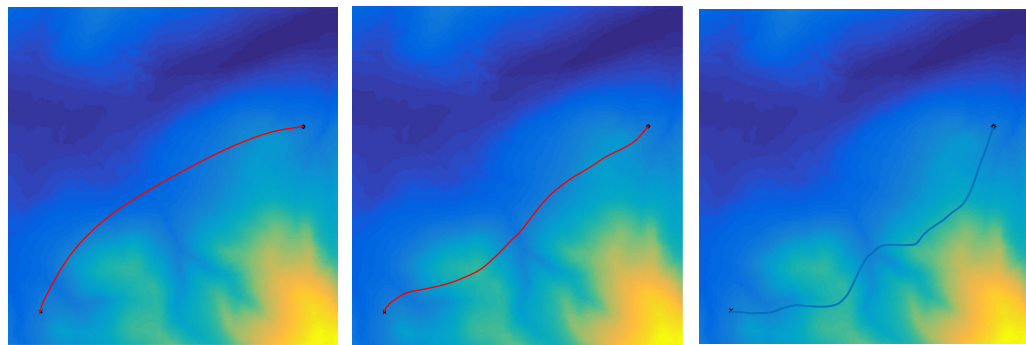


Fig. 11. Influence of sand landslides. Correction of the path according to the vector field given by the slope of the surface. Orthogonal mesh. Left: Without vector field. Middle: Vector field equal to the gradient. Right: The vector field is ten times the gradient.

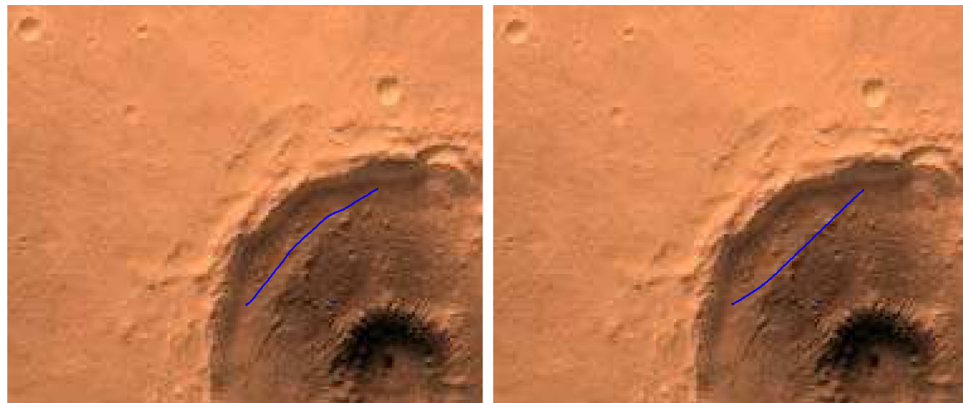


Fig. 12. Two different paths in the Gale crater. Lateral sand landslides proportional to the gradient. Orthogonal mesh. Left: Without landslides; Right: With landslides.

The scalar product is normalized to be in the interval [0, 1]. After that, different weights could be given to this component. Navigation in zones with more significant slopes is penalized.

Different vector fields are applied in Fig. 11 to test this parameter. Eq. (13) is used for the vectorial component of the cost. In this case, the scalar variable that is included in the cost is also the change in height with respect to the initial reference. A scale from dark blue to yellow is utilized to represent the height (yellow is the mountain peak). Fig. 11 (left) shows that, without the vector field, the planning module returns a smooth path that does not take into account possible sand landslides. When the external field is added to the cost value of each cell, the path is corrected to avoid zones with significant slopes. In this way, the rover will minimize the impact of sand landslides. Different paths are obtained depending on the weight given to the vector field. This option is not possible when using the AFM method because the vector field component is normalized. The path will not depend on the magnitude of the vector field. The vector field is utilized here to correct the path improving the safety of the vehicle.

In the left part of the figure, the path minimizes changes in height, but the robot is navigating in areas with important slopes that can cause the deterioration of the path due to landslides. This factor is corrected in the other cases. The changes in height are not minimized, but the path is flatter.

A different option that is studied in the second experiment is to use the external vector field to estimate the actual path that the robot will follow. In this experiment, the external vector field is utilized to compute how the presence of sand landslides affects the robot's path (Eq. (9) is applied again). After that, deviations could be corrected if necessary. Fig. 12 displays two different paths in the Gale crater taking into consideration the lateral sand landslides. The vector field that is created is proportional to the gradi-

ent of the surface. In the left part of the figure, a smooth path is computed without the external vector field. In the right part, the path is changed when sand landslides are taken into account. The scalar cost value is $H_{c_{ij}}$.

After analyzing the influence of the vector field, the planning module could correct the path if necessary. For example, an external vector field in the opposite direction could be added in order to obtain an actual path closer to the original one (left part of the figure).

5.2.2. Influence of scalar parameters

In this section, the aim is to test how to combine different options in the scalar cost function. The FMVF method is run for a triangular mesh (built from the original map in order to represent more accurately the three-dimensional surface) surrounding the Gale crater. The external vector field has been omitted for simplicity. The original map is transformed to a triangular surface with different heights, as can be appreciated in Fig. 13. The scale goes from white (lower altitude) to brown (crater peaks). The starting point is red and the goal is blue. Four different options are presented in the figure.

If the objective is to penalize only the inclination of the surface, the scalar cost should be $F_{scal,ij} = 1 - S_{t_{ij}}$. This option is illustrated in the upper right part of the figure. The Mars rover traverses the flat area given by the white triangles, which corresponds to the smallest gradients.

In the upper left part of the figure, the navigation module minimizes changes in height with respect to the initial point ($F_{scal,ij} = 1 - H_{c_{ij}}$). The rover navigates through zones with the same color trying to keep a constant height.

When only the spherical variance is included in the cost value ($F_{scal,ij} = 1 - S_{v_{ij}}$), the robot avoids obstacles such as rocks. This

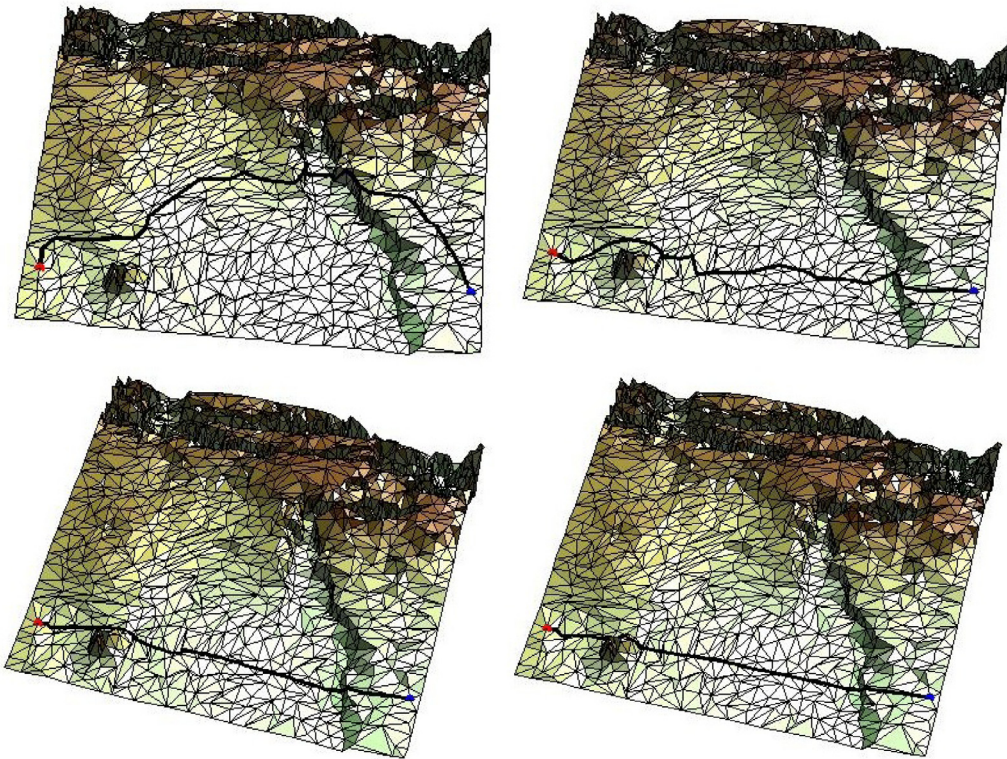


Fig. 13. Paths depending on $F_{scal,ij}$. Upper left: Height changes ($F_{scal,ij} = 1 - H_{cij}$); Upper right: Slope ($F_{scal,ij} = 1 - S_{tij}$); Bottom left: Spherical variance ($F_{scal,ij} = 1 - H_{cij}$); Bottom right: Combination ($F_{scal,ij} = 1 - (0.4 \cdot S_{vij} + 0.4 \cdot S_{tij} + 0.2 \cdot H_{cij})$).

case is detailed in the bottom left part of the figure. It can be considered that the path is not safe enough because the vehicle drives close to the mountain situated in the bottom left corner of the image. However, the reader has to notice that the scale of this map is huge because the information provided by sensors represents the whole surface of Mars (resolution of 60 km at the equator). The rover is actually kilometres away from the mountain. This fact led us to conclude that the spherical variance is a parameter that will be more important in smaller local maps.

An empirical combination of weights is set to compute the path shown in the bottom right part of the figure. These weights can be selected depending on the limitations of the rover or the features of interest.

It is also important to say that the initial solution calculated by the FMVF method can be seen as a tentative path for the robot. This path can be modified online depending on the sensor information.

5.3. Penalization according to missing information

An experiment where the flexibility of the method is demonstrated is presented in this section. The uncertainty about some zones can be estimated depending on the information provided by sensors. Following this idea, the velocity in some zones could be reduced or the dangerous regions could be avoided. For example, it could be interesting to penalize those areas where there is no visual information. In the FMVF technique, any factor can be taken into account if it can be included in the cost value.

It can be considered that there is not enough information to navigate in those zones with a lower height when compared to the initial point reference. If the rover is equipped with cameras, the interior of a crater could be unknown. Fig. 14 shows an example where the scalar cost is based on the changes with respect to the initial height. In addition, the cost is penalized if the height is

lower than the height of the initial point. This concept is implemented by introducing an extra variable in the scalar component of the cost function.

The paths are in the upper part of the figure. The potential fields are at the bottom. Dark blue is used for the locations with the worst potential. In the left part, a small penalty factor is given to the lower zones. In the right part, the potential of the lower regions is strongly penalized. The penalty factor can also be seen as a uncertainty measure about the sensor information.

As can be seen in the right part, the Mars rover avoids the lower regions in a safe way. When the penalty factor is small (left), it is not possible to navigate always in the safe zone.

The same concept can be applied to penalize the gradient or the spherical variance. An example with the slope is displayed in Fig. 15. In this case, the original scalar cost only includes the minimization of the slope and a penalty factor is introduced according to the slope. In other words, the scalar cost value is strongly penalized for big slopes. From a physical point of view, the idea is to navigate avoiding craters. The normalized gradient is given in Fig. 16.

In the left part of the figure, the path without the penalty factor is shown. Since the planning method minimizes the sum of the gradients, there are some situations (like this one) in which the path includes zones where the navigation is not completely safe. It can be appreciated that the rover enters a crater marked with an orange circle in the figure. The penalty factor makes sense in this case. In the right part, the rover does not enter the crater and the safety of the vehicle is improved.

6. Conclusions

Mars rovers require expert and intelligent systems to survive when exploring a hostile planet. In this paper, we have implemented a path planning method for Mars rovers that relies on a

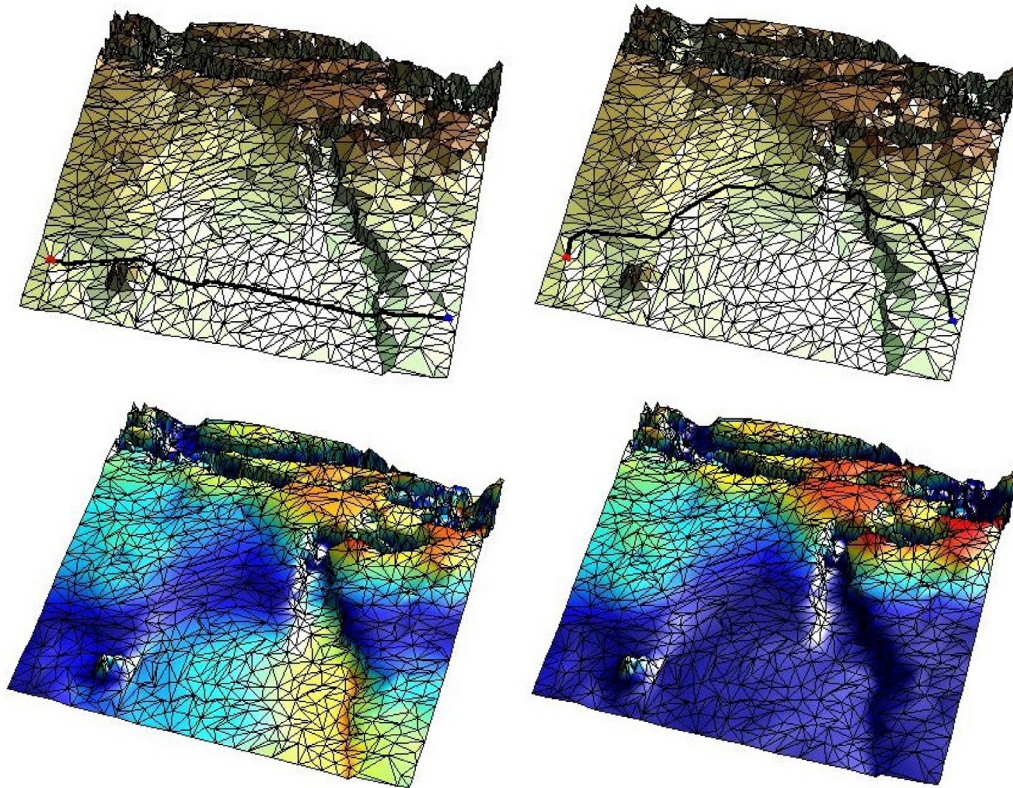


Fig. 14. Difference between paths when the scalar cost is penalized in the lower heights. Top: paths from initial location (red) to goal (blue); Bottom: Potential fields; Left: Small penalty factor; Right: Big penalty factor. (For interpretation of the references to colour in this figure legend, the reader is referred to the web version of this article.)

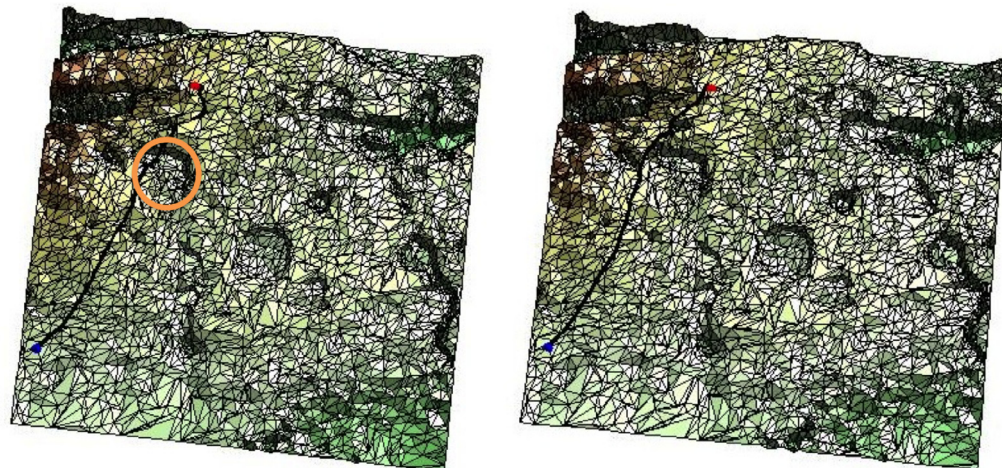


Fig. 15. Difference between paths when the scalar cost is penalized depending on the slope. Paths from initial location (red) to goal (blue). Left: No penalization; Right: Penalty factor for slopes bigger than a threshold (30 degrees). (For interpretation of the references to colour in this figure legend, the reader is referred to the web version of this article.)

modified version of the FM algorithm. The objective is to take into account the most common factors that can influence the vehicle when exploring the planet's surface. In our approach, these factors are classified into scalar and vectorial variables. In order to introduce these characteristics in the path planning module, a technique that optimizes a scalar cost function subjected to an external vector field is proposed.

The surface roughness, the slope of the terrain, and the changes in height with respect to the initial point of the path are the variables that are included in the scalar cost value. Any other feature defined by a scalar value could be added. In addition, these char-

acteristics can be combined in different ways in order to satisfy different requirements.

The planning strategy is also subjected to an external vector field that symbolizes phenomena like sand landslides. The influence of an external factor represented by a vector field on the velocity of the vehicle depends on the magnitude of both variables and the angle between them. To the best of our knowledge, it is the first time that a vector field is applied when designing a planning method for planet exploration.

The algorithm has been tested using simulated and real input data. Since different parameters can be introduced in the cost

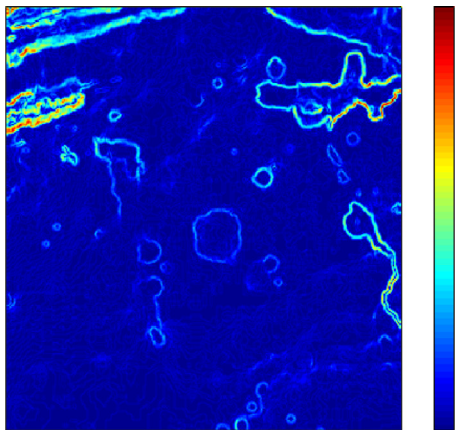


Fig. 16. Gradient of the surface for the map given in Fig. 15. Absolute values. Normalized between zero (blue) and one (red). Size: 300 × 300 cells. (For interpretation of the references to colour in this figure legend, the reader is referred to the web version of this article.)

function, the experiments validate our method under different circumstances that result in different cost values in order to highlight particular situations that can occur on Mars. The versatility of the method is one of the most important advantages of the current work. The planning module maintains the smoothness and the safety, characteristics that are reported in our previous work.

One of the main contributions is the development of a planning method that takes into account variables that can be modeled by a vector field. Two particular experiments have been carried out to simulate sand landslides. The influence of the landslide is minimized in the first one. In the second one, it is possible to estimate deviations in the path that can be corrected if necessary.

An interesting work to be accomplished in the future is to test different parameters in the cost function. For example, the solar energy could be included in the scalar component. The energy absorption (parameter to be optimized) depends on the angle between the normal to the solar panels and the vector from the rover to the sun. More direct sunlight reaches the panel for smaller angles.

References

- Barraquand, J., B. B. L., & Latombe, J. C. (1992). Numerical potential field techniques for robot path planning. *IEEE Transactions on Systems, Man, and Cybernetics*, 22(2), 224–241.
- Berg, M. D., Kreveld, M. V., Overmars, M., & Schwarzkopf, O. C. (2000). Computational geometry. In *Computational geometry* (pp. 1–17). Springer.
- Bougleux, S., Peyré, G., & Cohen, L. (2008). Anisotropic geodesics for perceptual grouping and domain meshing. In *European conference on computer vision* (pp. 129–142). Springer.
- Carsten, J., Rankin, A., Ferguson, D., & Stentz, A. (2007). Global path planning on board the mars exploration rovers. In *2007 IEEE aerospace conference* (pp. 1–11). IEEE.
- Castejón, C., Boada, B. L., Blanco, D., & Moreno, L. (2005). Traversable region modeling for outdoor navigation. *Journal of Intelligent and Robotic Systems*, 43(2–4), 175–216.
- Ferguson, D., & Stentz, A. (2006). Using interpolation to improve path planning: The field d* algorithm. *Journal of Field Robotics*, 23(2), 79–101.
- Garrido, S., Moreno, L., Abderrahim, M., & Blanco, D. (2009). FM²: A real-time sensor-based feedback controller for mobile robots. *International Journal of Robotics and Automation*, 24(1), 3169–3192.
- Garrido, S., Moreno, L., & Blanco, D. (2008). Exploration of a cluttered environment using voronoi transform and fast marching method. *Robotics and Autonomous Systems*, 56(12), 1069–1081.
- Ge, S. S., & Cui, Y. J. (2000). New potential functions for mobile robot path planning. *IEEE Transactions on Robotics and Automation*, 16(5), 615–620.
- Gennery, D. B. (1999). Traversability analysis and path planning for a planetary rover. *Autonomous Robots*, 6(2), 131–146.
- Ishigami, G., Nagatani, K., & Yoshida, K. (2007). Path planning for planetary exploration rovers and its evaluation based on wheel slip dynamics. In *Proceedings 2007 IEEE international conference on robotics and automation* (pp. 2361–2366). IEEE.
- Jbabdi, S., Bellec, P., Toro, R., Daunizeau, J., Pélégri-Issac, M., & Benali, H. (2008). Accurate anisotropic fast marching for diffusion-based geodesic tractography. *Journal of Biomedical Imaging*, 2008, 2.
- Kavraki, L. E., Svestka, P., Latombe, J.-C., & Overmars, M. H. (1996). Probabilistic roadmaps for path planning in high-dimensional configuration spaces. *IEEE Transactions on Robotics and Automation*, 12(4), 566–580.
- Kimmel, R., & Sethian, J. A. (1998). Computing geodesic paths on manifolds. *Proceedings of the National Academy of Sciences*, 95(15), 8431–8435.
- Kuffner, J. J., & LaValle, S. M. (2000). RRT-connect: An efficient approach to single-query path planning. In *Robotics and automation, 2000. Proceedings. ICRA'00. IEEE international conference on*: 2 (pp. 995–1001). IEEE.
- Laubach, S. L., & Burdick, J. W. (1999). An autonomous sensor-based path-planner for planetary microrovers. In *Robotics and automation, 1999. Proceedings. 1999 IEEE international conference on*: 1 (pp. 347–354). IEEE.
- LaValle, S. M. (2006). *Planning algorithms*. Cambridge University Press.
- LaValle, S. M. (2011). Motion planning. *IEEE Robotics and Automation Magazine*, 18(1), 79–89.
- Maimone, M. W., Leger, P. C., & Biesiadecki, J. J. (2007). Overview of the mars exploration rovers? autonomous mobility and vision capabilities. *IEEE international conference on robotics and automation (ICRA) space robotics workshop*.
- Muñoz, P., Rodríguez, M. D., Castaño, B., & Martínez, A. (2012). Fast path-planning algorithm for future mars exploration. *International symposium on artificial intelligence, robotics and automation in space*. Turin.
- Osher, S., & Sethian, J. A. (1988). Fronts propagating with curvature-dependent speed: Algorithms based on hamilton-Jacobi formulations. *Journal of Computational Physics*, 79(1), 12–49.
- Pardeiro, J. (2015). *Trajectory planning algorithms based on fast marching square*. Carlos III University of Madrid Master's thesis.
- Petres, C., Pailhas, Y., Patron, P., Petillot, Y., Evans, J., & Lane, D. (2007). Path planning for autonomous underwater vehicles. *IEEE Transactions on Robotics*, 23(2), 331–341.
- Petres, C., Pailhas, Y., Petillot, Y., & Lane, D. (2005). Underwater path planing using fast marching algorithms. In *Europe oceans*: 2 (pp. 814–819). IEEE.
- Peyré, G. (2010). Advanced signal, image and surface processing. Ceremade, University Paris-Dauphine.
- Potiris, S., Tompkins, A., & Goktogan, A. (2014). Terrain-based path planning and following for an experimental mars rover. In *Australasian conference on robotics and automation, Melbourne* (pp. 1–10).
- Rekleitis, I., Bedwani, J. L., Dupuis, E., & Allard, P. (2008). Path planning for planetary exploration. In *Computer and robot vision, 2008. CRV'08. Canadian conference on* (pp. 61–68). IEEE.
- Sethian, J. A. (1996). Theory, algorithms and applications of level set methods for propagating interfaces. *Acta Numerica*, 5, 309–395.
- Sethian, J. A., & Vladimirsky, A. (2003). Ordered upwind methods for static hamilton-Jacobi equations: Theory and algorithms. *SIAM Journal on Numerical Analysis*, 41(1), 325–363.
- Shum, A., Morris, K., & Khajepour, A. (2015). Direction-dependent optimal path planning for autonomous vehicles. *Robotics and Autonomous Systems*, 70, 202–214.
- Valero-Gómez, A., Gómez, J. V., Garrido, S., & Moreno, L. (2013). The path to efficiency: Fast marching method for safer, more efficient mobile robot trajectories. *IEEE Robotics and Automation Magazine*, 20(4), 111–120.
- Volpe, R., Estlin, S., Laubach, S., Olson, C., & Balaram, J. (2000). Enhanced mars rover navigation techniques. In *Robotics and automation, 2000. Proceedings. ICRA'00. IEEE international conference on*: 1 (pp. 926–931). IEEE.
- Yatziv, L., Bartesaghi, A., & Sapiro, G. (2006). O (n) implementation of the fast marching algorithm. *Journal of Computational Physics*, 212(2), 393–399.